Enhanced quantum dot optical down-conversion using asymmetric 2D photonic crystals

Fuchyi Yang* and Brian T. Cunningham

Nano Sensors Group, Department of Electrical and Computer Engineering,
University of Illinois at Urbana-Champaign,
Micro and Nanotechnology Laboratory, 208 N Wright St, Urbana, Illinois 61801, USA
**fyang5@illinois.edu*

Abstract: Asymmetric 2D photonic crystals were fabricated using polymer embedded PbS quantum dots on plastic substrates for enhancing optical down conversion efficiency from blue to near infrared wavelengths through enhanced extraction and excitation effects. We demonstrate 8x improvement of QD emission at normal incidence extraction from enhanced extraction and 2.5x improvement in power conversion efficiency from enhanced excitation.

OCIS codes: (050.5298) Photonic crystals; (220.4241) Nanostructure fabrication

References and links

1. D. Graham-Rowe, "From dots to devices," Nat. Photonics **3**(6), 307–309 (2009).
2. V. Sukhovatkin, S. Hinds, L. Brzozowski, and E. H. Sargent, "Colloidal quantum-dot photodetectors exploiting multiexciton generation," Science **324**(5934), 1542–1544 (2009).
3. S. A. McDonald, G. Konstantatos, S. G. Zhang, P. W. Cyr, E. J. D. Klem, L. Levina, and E. H. Sargent, "Solution-processed PbS quantum dot infrared photodetectors and photovoltaics," Nat. Mater. **4**(2), 138–142 (2005).
4. V. Aroutiounian, S. Petrosyan, A. Khachatryan, and K. Touryan, "Quantum dot solar cells," J. Appl. Phys. **89**(4), 2268–2271 (2001).
5. S. Giménez, I. Mora-Seró, L. Macor, N. Guijarro, T. Lana-Villarreal, R. Gómez, L. J. Diguna, Q. Shen, T. Toyoda, and J. Bisquert, "Improving the performance of colloidal quantum-dot-sensitized solar cells," Nanotechnology **20**(29), 295204 (2009).
6. P. O. Anikeeva, J. E. Halpert, M. G. Bawendi, and V. Bulović, "Quantum dot light-emitting devices with electroluminescence tunable over the entire visible spectrum," Nano Lett. **9**(7), 2532–2536 (2009).
7. N. Tessler, V. Medvedev, M. Kazes, S. H. Kan, and U. Banin, "Efficient near-infrared polymer nanocrystal light-emitting diodes," Science **295**(5559), 1506–1508 (2002).
8. V. Wood, M. J. Panzer, J. L. Chen, M. S. Bradley, J. E. Halpert, M. C. Bawendi, and V. Bulovic, "Inkjet-Printed Quantum Dot-Polymer Composites for Full-Color AC-Driven Displays," Adv. Mater. (Deerfield Beach Fla.) **21**(21), 2151–2155 (2009).
9. K. S. Cho, E. K. Lee, W. J. Joo, E. Jang, T. H. Kim, S. J. Lee, S. J. Kwon, J. Y. Han, B. K. Kim, B. L. Choi, and J. M. Kim, "High-performance crosslinked colloidal quantum-dot light-emitting diodes," Nat. Photonics **3**(6), 341–345 (2009).
10. D. Englund, D. Fattal, E. Waks, G. Solomon, B. Zhang, T. Nakaoka, Y. Arakawa, Y. Yamamoto, and J. Vucković, "Controlling the spontaneous emission rate of single quantum dots in a two-dimensional photonic crystal," Phys. Rev. Lett. **95**(1), 013904 (2005).
11. M. Barth, A. Gruber, and F. Cichos, "Spectral and angular redistribution of photoluminescence near a photonic stop band," Phys. Rev. B **72**(8), 085129 (2005).
12. F. S. Diana, A. David, I. Meinel, R. Sharma, C. Weisbuch, S. Nakamura, and P. M. Petroff, "Photonic crystal-assisted light extraction from a colloidal quantum dot/GaN hybrid structure," Nano Lett. **6**(6), 1116–1120 (2006).
13. N. Ganesh, I. D. Block, P. C. Mathias, W. Zhang, E. Chow, V. Malyarchuk, and B. T. Cunningham, "Leaky-mode assisted fluorescence extraction: application to fluorescence enhancement biosensors," Opt. Express **16**(26), 21626–21640 (2008).
14. N. Ganesh, W. Zhang, P. C. Mathias, E. Chow, J. A. N. T. Soares, V. Malyarchuk, A. D. Smith, and B. T. Cunningham, "Enhanced fluorescence emission from quantum dots on a photonic crystal surface," Nat. Nanotechnol. **2**(8), 515–520 (2007).
15. I. V. Soboleva, E. Descrovi, C. Summonte, A. A. Fedyanin, and F. Giorgis, "Fluorescence emission enhanced by surface electromagnetic waves on one-dimensional photonic crystals," Appl. Phys. Lett. **94**(23), 231122 (2009).
16. F. Yang, G. Yen, and B. T. Cunningham, "Voltage-tuned resonant reflectance optical filter for visible wavelengths fabricated by nanoreplica molding," Appl. Phys. Lett. **90**(26), 261109 (2007).

#139110 - $15.00 USD Received 3 Dec 2010; revised 3 Feb 2011; accepted 9 Feb 2011; published 14 Feb 2011

17. F. Yang, G. Yen, and B. T. Cunningham, "Integrated 2D photonic crystal stack filter fabricated using nanoreplica molding," Opt. Express **18**(11), 11846–11858 (2010).
18. www.srubiosystems.com.
19. I. D. Block, L. L. Chan, and B. T. Cunningham, "Photonic crystal optical biosensor incorporating structured low-index porous dielectric," Sens. Actuators B Chem. **120**(1), 187–193 (2006).
20. N. Ganesh, I. D. Block, and B. T. Cunningham, "Near ultraviolet-wavelength photonic-crystal biosensor with enhanced surface-to-bulk sensitivity ratio," Appl. Phys. Lett. **89**(2), 023901 (2006).
21. J. J. Peterson, and T. D. Krauss, "Photobrightening and photodarkening in PbS quantum dots," Phys. Chem. Chem. Phys. **8**(33), 3851–3856 (2006).

1. Introduction

Colloidal semiconductor quantum dots (QD) are solution processed nanometer sized particles [1]. Due to the quantum confinement effect of the electronic wave function, QD exhibit discrete electron energy levels which lead to narrow absorption and emission bands which are blue shifted from their bulk counterparts. Varying the size and materials of the QD enables tuning of the emission and absorption wavelengths from the ultraviolet (UV) to the near infrared (NIR). QD are now routinely incorporated into a broad range of photonic emitters and detectors including photoconductors [2,3], solar cells [4,5], LEDs [6,7], and video displays [8,9] for their unique optical properties. Engineering the emission characteristics of QD would enhance the performance of these photonic devices and potentially enable new applications. Moreover, colloidal QD are synthesized in solution in large quantities, which make them an ideal choice as light emitters for incorporation into large area photonic devices through either spincoating or printing. Photonic crystals (PC) have been demonstrated to allow versatile control over optical properties of QD. Increasing the radiative emission rate [10], modifying the angular and spectral emission distribution [11,12], and enhancing the emission intensity [12–15]from QD have been shown. This work presents a PC enabled enhancement of optical down conversion through enhanced excitation of $\lambda = 450$ nm light and enhanced extraction of NIR light in the $\lambda = 800$-900 nm range. Nanoreplica molding, which is compatible with large area and flexible substrates, is used to fabricate the PC devices on plastic substrates [16,17]. The ability to make devices on flexible substrates extends the potential applications over traditional fabrication methods such as photolithography and electron beam lithography. Additionally, nanoreplica molding has been incorporated into a roll-to-roll large scale manufacturing process of optical biosensors [18]. The PC devices discussed in this work could potentially be used as efficient NIR light sources through incorporation into a LED which is used for optical pumping of the QD layer. In addition, potential large area applications include NIR planar lighting and NIR displays by incorporating a large area PC with a backlight as an optical pump. The ability to fabricate flexible and lightweight NIR light sources improves portability and their incorporation onto non-planar surfaces.

A 2D asymmetric PC was designed and fabricated in order to modify the emission characteristics of colloidal lead sulfide (PbS) QD interacting with the PC environment. The PC was used to engineer the optical dispersion and spatial profile of optical modes supported within the PC structure through design of the PC period, modulation depth, duty cycle, and refractive index (RI). Moreover, optical modes which exist above the light line are leaky modes due to the fact that they can be coupled into and out of the PC through free space propagating waves enabled by phase matching through the PC. This coupling is strictly determined by the wavelength and incident/emission angle of the incoming/outgoing light [13]. In essence, the PC behaves as an optical antenna which redirects emitted light in a controlled direction. Therefore, it is possible to engineer the PC to efficiently extract light at desired wavelengths and emission angles. In addition, light of a particular wavelength and incident angle can be resonantly coupled into the PC structure in order to excite a PC mode with an electric field intensity much higher than the incident field. 1D PC and symmetric 2D PC are limited in the achievable wavelength separation of their leaky modes. In order to design a PC with simultaneous leaky modes at $\lambda = 450$ nm and $\lambda = 800$-900 nm, an asymmetric 2D PC design was chosen. Through the enhanced extraction and enhanced

#139110 - $15.00 USD Received 3 Dec 2010; revised 3 Feb 2011; accepted 9 Feb 2011; published 14 Feb 2011

excitation effects, a 2D asymmetric PC with embedded PbS QD demonstrated enhanced efficiency of optical down conversion from the blue to NIR wavelengths.

2. Design

The 2D surface PC is designed asymmetrically such that the period of RI modulation differs in orthogonal directions. This design produces a 2D surface PC that behaves as two combined 1D surface PCs. The 2D surface PC design, shown in Fig. 1, is comprised of a 2D rectangular lattice of holes that are d = 130 nm deep. One direction of the surface PC has a period of Λ_2 = 220 nm with 50% duty cycle while the orthogonal direction has a period of Λ_1 = 520 nm with 60% duty cycle. A high RI region, with thickness t = 100 nm, is surrounded by lower RI regions in order to support guided PC modes. The optical properties of the device are simulated using rigorous coupled wave analysis (DiffractMod, RSOFT) which provides solutions to Maxwell's equations for periodic structures. The simulation region is a single period of the PC structure with periodic boundary conditions in both *x* and *y* directions. The PC is a three layer structure with a high RI layer surrounded above and below by two low RI layers. A thermoplastic polymer was used as the low RI layer while the high RI layer was simulated as titanium dioxide (TiO_2). In order to take into account the material dispersion, the simulation was run with different RI values at λ = 450 nm and λ = 800-900 nm. The RI values were obtained from measurements of thin film samples of the corresponding materials using a variable angle spectroscopic spectrometer (J. A. Woollam). As mentioned above, leaky modes of the PC are coupled through free space incident light. It is known that this phenomena results in resonant reflection peaks in the reflection spectrum of the incident light through the guided mode resonance effect [19,20]. Moreover, varying the angle of incident light allows coupling to leaky modes of varying propagation constants through phase matching from the PC. As a result, the PC band diagram is obtained through measurement of the reflection of the PC as a function of both incident angle and wavelength. Additionally, the leaky modes' polarization is dependent on the polarization of the coupled incident light.

It is possible to design a 2D asymmetric surface PC to engineer modes with wide wavelength separation in order to enhance optical down conversion from the blue to NIR wavelengths. In the PC band diagram shown in Fig. 2(b), both TE and TM modes are present in the NIR wavelength range of λ = 800-900 nm which spectrally overlap with the NIR emission of the PbS QD. Thus, this provides enhanced extraction of emitted light from QD through coupling of the PC mode to free space. Additionally, as seen in Fig. 2(a), PC modes are also obtained at λ = 450 nm which spectrally overlap with the blue wavelength pump light, providing enhanced excitation through resonant coupling of the excitation light into the PC mode.

#139110 - $15.00 USD Received 3 Dec 2010; revised 3 Feb 2011; accepted 9 Feb 2011; published 14 Feb 2011

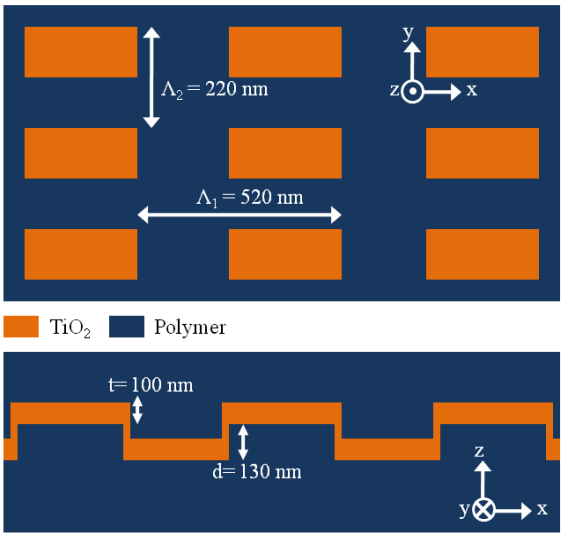

Fig. 1. Top and side cross section schematic view of the 2D asymmetric photonic crystal. The period is Λ_1 = 520 nm in *x* direction and Λ_2 = 220 nm in *y* direction. Modulation depth is d = 130 nm and TiO_2 thickness is 100 nm.

The simulated electric field mode profiles of the TE mode at λ = 888 nm and TM mode at λ = 848 nm are shown in Fig. 3(a) and Fig. 3(b), respectively. The white rectangular regions depict the high RI TiO_2 material. In this simulation, the QD are located in the polymer. Due to the boundary conditions of continuous dielectric displacement, the TM mode has higher electric field intensity concentrated in the low RI regions as compared to the TE mode. Additionally, the TM mode has electric field components in both *x* (not shown) and *z* directions, while the TE mode only has electric field components in the *y* direction.

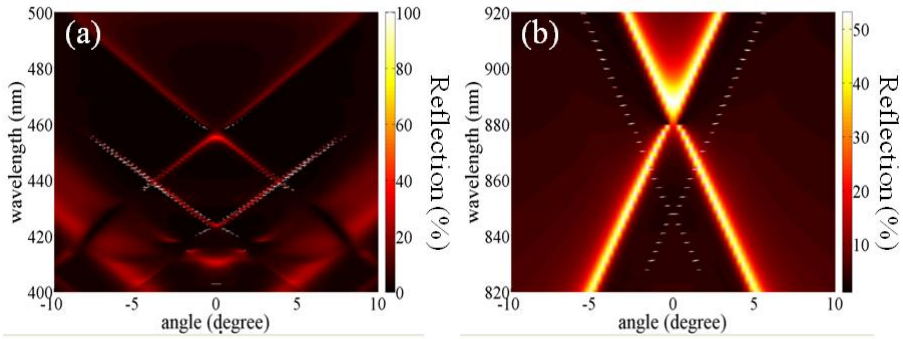

Fig. 2. RWCA simulation results of the PC leaky mode band diagram at (a) excitation wavelength range and (b) extraction wavelength range.

The PC mode at λ = 850 nm does not interact with the Λ_2 = 220 nm PC since the feature sizes are much smaller the wavelength of the light. However, the PC mode at λ = 450 nm does interact with the Λ_1 = 520 nm PC since the feature sizes are larger than the wavelength of the light. This interaction causes diffraction from the Λ_1 = 520 nm PC which reduces the coupling efficiency which was confirmed by simulation results. This effect can be minimized by varying the duty cycle of the Λ_1 = 520 nm PC to the optimal value of 60% resulting in a maximum reflection efficiency of 80% for the PC mode at λ = 450 nm. Maximizing this value is critical in obtaining the highest intensity electric field for enhanced excitation.

#139110 - $15.00 USD Received 3 Dec 2010; revised 3 Feb 2011; accepted 9 Feb 2011; published 14 Feb 2011

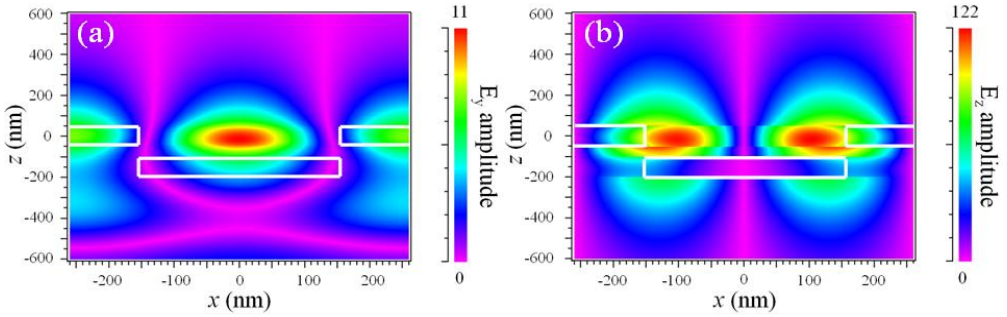

Fig. 3. RWCA simulations of (a) TE mode *y*-polarized electric field at λ = 888 nm and (b) TM mode *z*-polarized electric field at λ = 848 nm.

3. Fabrication

The fabrication process employs nanoreplica molding which allows room temperature, low cost, and large area fabrication on plastic substrates. The process flow diagram is depicted in Fig. 4. First, a 2D surface PC structure was nanoreplica molded from a master wafer onto a polyethylene terephthalate (PET) substrate. The master is a 2-inch diameter silicon wafer upon which a 2D surface PC structure with a period of Λ_1 = 520 nm and 50% duty cycle and Λ_2 = 220 nm and a 60% duty cycle is patterned by electron beam lithography over a 2x2 mm^2 area. The 2D surface PC pattern is etched into the silicon wafer to a depth of d = 130 nm by reactive ion etching. The completed master wafer is composed of a rectangular lattice of rectangular posts. Figure 5(a) shows an SEM of the silicon master. The 2D surface PC is nanoreplica molded from a thermoplastic embedded with QD. 10 mg of the thermoplastic (Tetramer NDM, Tetramer Tech.) is dissolved in 100μL of the organic solvent, mesitylene, while the PbS QD (Evident Tech.) are in a toluene solution of 10mg/mL concentration. 100 μL thermoplastic solution and 400 μL QD solution are mixed to obtain a mass ratio of QD/thermoplastic of 2/5. The mixture is placed in a desiccator in order to evaporate the solvent until 100 μL remains. This solution of thermoplastic/QD is spin-coated onto the silicon master wafer at 3000 rpm for 30 seconds. A thin film of approximately 4 μm of the thermoplastic forms on the silicon master wafer and conforms to the 2D surface PC structure. The silicon master is then placed on a hotplate at 110°C for 120 seconds in order to evaporate any remaining solvent. The nanoreplica mold of the PC structure is then transfer printed onto a flexible PET substrate. In order to transfer the PC structure from the silicon master, a layer of liquid ultraviolet curable polymer (UVCP) was drop coated over the thermoplastic/QD film. A PET substrate is then placed over the master wafer and brought into contact using mechanical pressure from a rolling cylinder. This enabled the UVCP drops to form a thin continuous layer between the PET and the thermoplastic/QD thin film. Next, the UVCP is cured for 90 seconds using a high intensity UV lamp (Xenon Corp.). The PET substrate, along with the UVCP layer and thermoplastic/QD thin film, is released from the silicon master and the thin film of thermoplastic/QD with the 2D surface PC nanoreplica mold is fabricated. Figure 5(b) shows an SEM image of the nanoreplica mold. In order to produce a surface PC that supports optical modes, a high RI thin film must be deposited over the low RI (n = 1.56) replica-molded grating structure. Sputter-deposited thin films of approximately t = 110 nm of TiO_2, with a RI of n = 2.59 at λ = 450 nm and n = 2.32 at λ = 850 nm, served as the high RI layer. Next, an additional film of thermoplastic/QD is spincoated over the TiO_2 layer in order to complete the device structure. After spincoating, the device is baked in an oven at 90°C for 15 minutes to evaporate any remaining solvents. Even though this work used a 2x2 mm^2 patterned area for proof of concept, the fabrication area is limited only by the size of the silicon master. Previous work using nanoreplica molding used an 8 inch diameter silicon master wafer to fabricate large area PC devices [16].

#139110 - $15.00 USD Received 3 Dec 2010; revised 3 Feb 2011; accepted 9 Feb 2011; published 14 Feb 2011

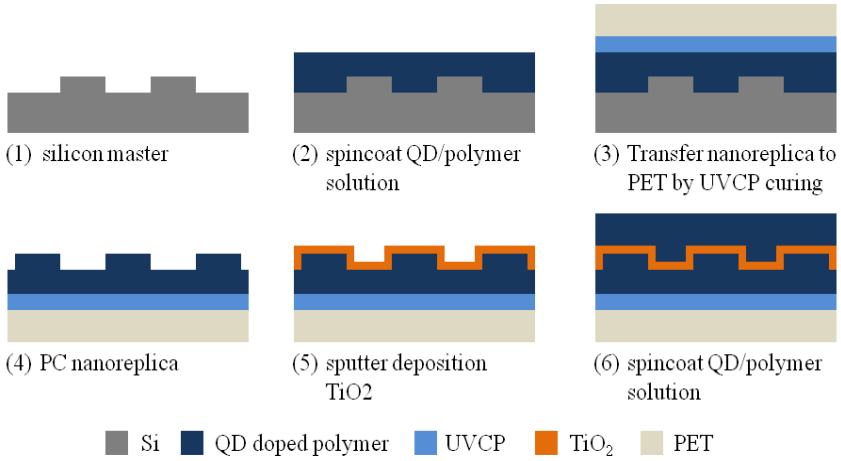

Fig. 4. Process flow diagram of nanoreplica molding process of 2D photonic crystal.

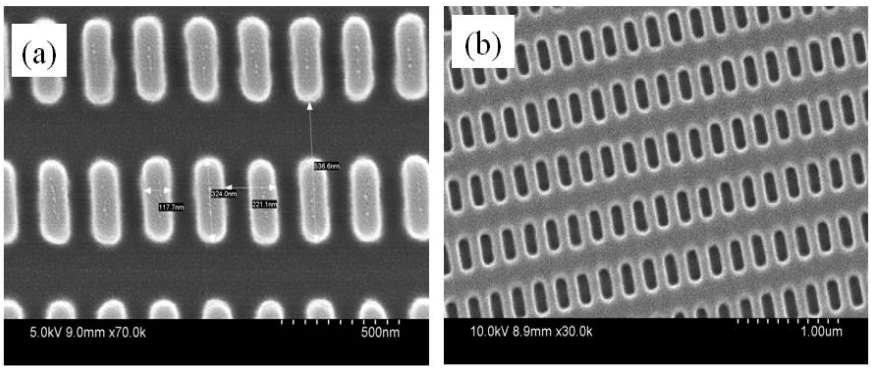

Fig. 5. SEM images of (a) silicon master from step (1) of Fig. 4 and (b) photonic crystal nanoreplica mold from step (4) of Fig. 4. No defects seen in SEM image of nanoreplica mold, and photonic crystal dimensions are well preserved from nanoreplica molding.

4. Enhanced extraction

The angle resolved fluorescence setup shown in Fig. 6 is used to characterize the emission properties of the PC device. A continuous wave (CW) laser source at $\lambda = 457$ nm is used to optically pump the QD. The PC device is mounted on an adjustable tilt mount that can rotate in order to adjust the incident angle between the PC and the excitation laser beam. A fiber optic cable connected to a collimating lens is attached to an optics rail that is allowed to rotate around the mount holding the PC device. The light emitted from the QD is collected at different extraction angles relative to the PC surface normal. The collimating lens is adjusted relative to the optical fiber end such that only light which is incoming at normal incidence is coupled into the fiber. This enabled the collection optics to have good angular resolution for observing emission of the QD. A high pass filter is placed in front of the collimating lens in order to filter out the excitation light at $\lambda = 457$ nm. The other end of the optical fiber is connected to a spectrometer (USB2000, Ocean Optics) and the emission spectrum is observed using the accompanying software (001Base, Ocean Optics). Using angle resolved fluorescence, the enhanced extraction effect is measured by setting the excitation angle θ constant at an off resonant value while varying the extraction angle φ from 0 to 10 degrees in 0.5 degree increments.

#139110 - $15.00 USD Received 3 Dec 2010; revised 3 Feb 2011; accepted 9 Feb 2011; published 14 Feb 2011

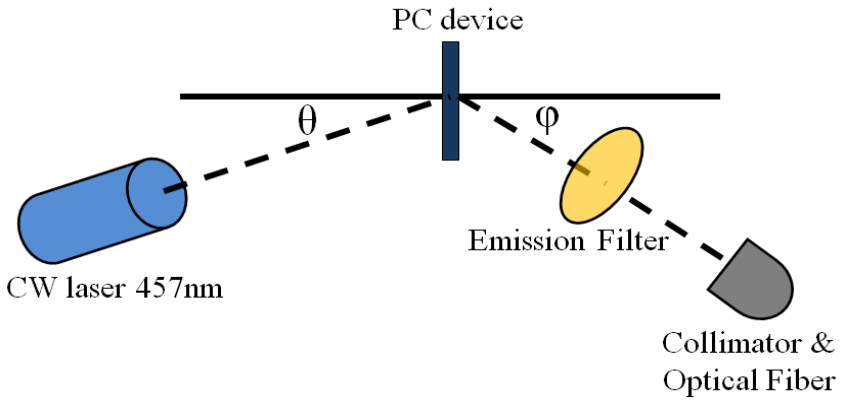

Fig. 6. Angle resolved fluorescence setup used to characterize the emission properties of QD in the PC device. The excitation angle θ and the extraction angle φ are both adjustable. Enhanced extraction experiment is performed by varying the extraction angle φ while keeping the excitation angle θ constant. Enhanced excitation experiment is performed by varying the excitation angle θ while keeping the extraction angle φ constant.

The photonic band diagram of the 2D PC can be experimentally obtained by acquiring the transmission spectrum at different incident angles and compiling the data to form a plot of the transmission as a function of both wavelength and angle. The optical transmission setup comprises a broadband tungsten-halogen lamp which is coupled to an optical fiber connected to a collimator. The light is incident on the PC, and the transmitted light is collected through another optical fiber coupled to a spectrometer (Ocean Optics USB2000). The PC is held on a rotation mount which enabled characterization of the transmission spectrum at varying incident angles. Using unpolarized light, the photonic band diagram for the PC is obtained and depicted in Fig. 7(a). Two offset "X" shaped features are seen in the photonic band diagram. The band labeled *i* is a wide full width half maximum (FWHM) TE band that is resonant at λ = 900 nm at normal incidence. Likewise, the band labeled *ii* is a narrow FWHM TM band that is resonant at λ = 860 nm at normal incidence. These are the leaky modes allowed by the surface PC. The experimental band diagram is red shifted by approximately $\Delta\lambda$ = 12 nm compared to the simulated band diagram in Fig. 2(a). This is due to slight differences between the simulated and fabricated structures due to fabrication variations. In addition, the RI dispersion of the materials comprising the PC was not taken into account, within the range of λ = 820 – 920 nm, in the simulation. However, even with the simplified simulated PC structure, the experimental and simulated results agreed quite well, qualitatively. The polarization dependence of the TE and TM bands was confirmed by placing linear polarizers in front of the collection optical fiber. The two bands could distinguished by a 90° rotation of the linear polarizer. When there is spatial and spectral overlap, the QD emission is preferentially coupled to these surface PC modes and the photons are coupled out of the surface PC to free space at the appropriate extraction angles which satisfy the phase matching condition. This is observed in the angle resolved emission measurements shown in Fig. 7(b). The emission intensity from the QD is much stronger along the bands of the surface PC due to this enhanced extraction effect.

The emission is strongest when the surface PC mode spectrally overlaps the emission peak of the QD at λ = 860 nm and decreases for wavelengths away from this value. In fact, the emission is much lower at wavelengths above λ = 900 nm and below λ = 800 nm. This is due to the poor spectral overlap between the QD emission spectrum and the PC optical modes outside this wavelength range. Additionally, the enhanced extraction effect is stronger for the TM band than the TE band. The TM mode has better spatial overlap with the low RI regions (thermoplastic/QD layers) of the PC where the QD are located, as shown in the simulations

#139110 - $15.00 USD Received 3 Dec 2010; revised 3 Feb 2011; accepted 9 Feb 2011; published 14 Feb 2011

results in Fig. 3(b). Thus, this improves the coupling of photons into the TM leaky modes, and point to the TM modes having higher extraction enhancement than the TE modes.

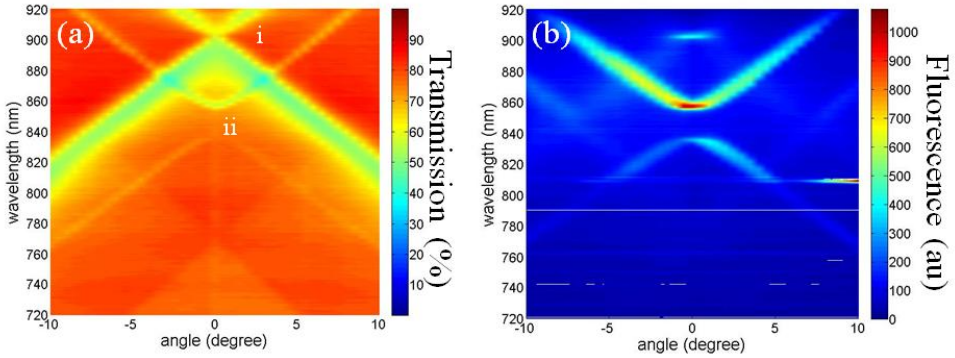

Fig. 7. (a) Experimental photonic band diagram for the PC device and (b) the corresponding angle resolved emission spectrum of QD in the PC device.

At normal incidence, the emission spectrum of QD within the surface PC (red curve) and QD with no surface PC (blue curve) are compared and shown in Fig. 8. The two shorter wavelength emission peaks correspond to extraction due to outcoupling from TM modes, while the longest wavelength emission peak corresponds to extraction enhancement due to outcoupling from a TE mode. At these wavelengths and normal incidence emission, the enhanced extraction effect is clearly seen over QD with no surface PC. At λ = 865 nm, the enhancement is ~8x relative to an adjacent QD/polymer coated surface with no PC pattern.

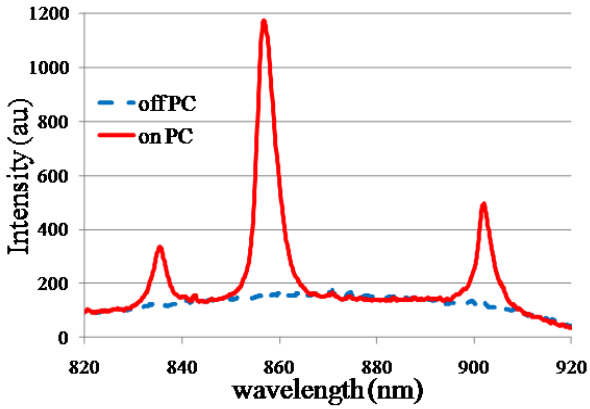

Fig. 8. Emission from QD at normal incidence extraction angle for QD in the PC device (red) and QD with no PC (blue). The enhanced extraction is about eight times at the emission peak of λ = 865 nm.

Angle resolved emission measurements are obtained for QD with no surface PC and compared to QD within a surface PC. The emission spectrum for QD with no surface PC shows no enhanced extraction effect and no variation in emission peak intensity as a function of angle. The QD within the surface PC show clear modifications in their emission characteristics in comparison. This effect is useful for controlling the emission angle of a narrow band of wavelengths in order to achieve better coupling or collection efficiency to other optical elements.

#139110 - $15.00 USD Received 3 Dec 2010; revised 3 Feb 2011; accepted 9 Feb 2011; published 14 Feb 2011

5. Enhanced excitation

Angle resolved emission measurements were also used to characterize the enhanced excitation effect of the PC. This was accomplished by observing the emission from the QD at a fixed extraction angle φ normal to the PC surface while varying the excitation angle θ. At a certain excitation angle, the pump light is able to couple into a PC mode through phase matching enabled by the PC. This results in enhanced electric fields relative to the pump light which increases the absorption rate of the QD. Consequently, the emission intensity is enhanced. Thus, at this resonant excitation angle, the QD emission intensity is at maximum. Figure 9 shows the transmission spectrum of a PC at 5.5° incident angle, along with the emission spectrum of the pump laser. There is good spectral overlap between the PC resonance and the pump light. Additionally, the polarization of the PC mode matches the polarization of the pump light which is critical for coupling. The measured resonance transmission efficiency is 47% as observed using the broadband transmission setup. Using a silicon photodetector to measure the transmitted power of the pump laser at different excitation angles result in a measured transmission efficiency of 40%. This discrepancy is most likely due to the limited resolution of the spectrometer.

The resolved emission intensity at normal incidence was observed as a function of excitation angle, and the maximum fluorescence intensity at λ = 856 nm was plotted as a function of the excitation angle. From Fig. 10, the enhanced excitation effect is shown to increase the fluorescence intensity 1.5x for the measured PC. Even though this demonstrates enhanced excitation, the enhancement value is limited by the coupling efficiency of the PC mode. The enhanced electric fields enabled through coupling to the PC mode are lowered due to multiple optical loss mechanisms. Currently, the transmission efficiency is 40% resulting in low enhancement values. Improving the transmission efficiency at the resonant wavelength, i.e. reducing the transmission value towards 0%, will result in higher excitation enhancement values. The main loss mechanisms are absorption from the QD and polymer and scattering from the PC. Since the excitation light at wavelength λ = 457 nm is able to interact with the λ = 550 nm period PC, this results in scattering and introduces loss to the PC mode. Thus, the efficiency is reduced resulting in lowered electric fields and a lower Q factor. Improving on the PC design to reduce this scattering loss will lead to higher excitation enhancement values.

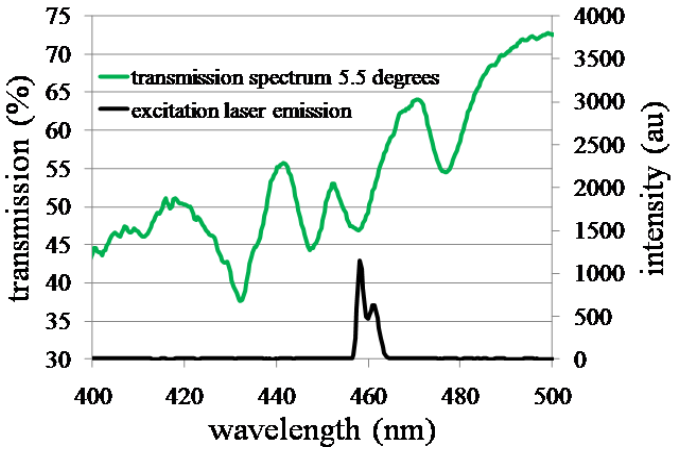

Fig. 9. Transmission spectrum of the PC device at 5.5 degrees oblique incidence overlaid with the emission laser of the excitation laser. Good spectral overlap is observed at λ = 457nm at this excitation angle which satisfies the enhanced excitation condition.

The conversion efficiency of the QD embedded PC was measured using an integrating sphere. The conversion efficiency is defined as the input power of the laser divided by the output power of the QD. This was measured using a silicon photodetector. The excitation

#139110 - $15.00 USD Received 3 Dec 2010; revised 3 Feb 2011; accepted 9 Feb 2011; published 14 Feb 2011

laser power was measured directly without the integrating sphere. The PC was placed directly in front of an input port of the integrating sphere and pumped using the excitation laser. An emission filter is placed in front of the photodetector and the QD emission was measured from the output port of the integrating sphere. This measured power was then converted into total power by taking into account the area ratio between the integrating sphere and the output port and also the fact that only half of the QD emission is directed into the integrating sphere while the other half is directed away.

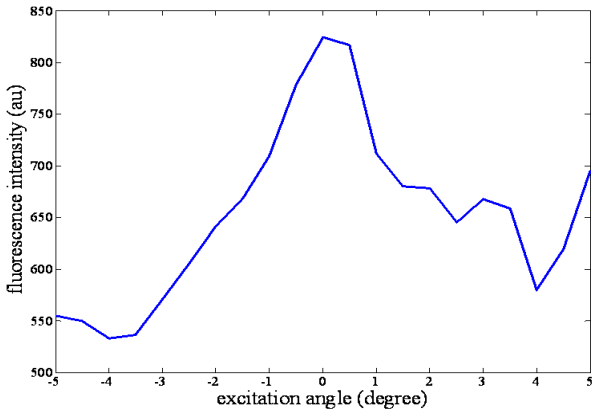

Fig. 10. Peak emission fluorescence intensity for λ = 856 nm at normal incidence extraction angle for varying excitation angle. An increase in fluorescence intensity is observed at the resonant excitation angle condition.

The measured conversion efficiency is comparable between QD embedded in a PC and QD embedded in non-structured polymer when enhanced excitation is absent. The enhanced extraction effect couples light into preferential directions and does not increase the spontaneous emission rate of the QD. Therefore, no increase in emission power is expected. Re-absorption effects might result in decreased emission power in the PC device compared to non structured polymer due to increased interaction time for the output light that couples to leaky modes for enhanced extraction. However, this was not seen in the experimental results indicating that re-absorption effects are negligible for this PC device. Typical conversion efficiencies for QD in non-structured polymer were around 10%. A non-reversible degradation in the conversion efficiency of PC devices was observed after being optically pumped over time. This was due to a non-reversible decrease in the emission intensity of the PbS QD over time, which is a characteristic of the QD and not a result of the PC design [21]. The conversion efficiency of the PC device was measured as a function of excitation angle. At non resonant excitation angle, the measured conversion efficiency was around 10% and comparable to QD in non-structured polymer. At the resonant excitation angle, enhanced excitation occurred, and the QD embedded in the PC increase in emission power due to increased absorption rate of the excitation light. An accompanying increase in conversion efficiency occurred. At the resonant angle, the enhanced excitation effect improved the conversion efficiency approximately 2.5x, from 10% to 25%, for QD embedded in PC compared to QD embedded in non-structured polymer layer as shown in Fig. 11. The differences in enhanced excitation values between Figs. 10 and 11 are due to Fig. 10 reporting enhancement values at a single wavelength while Fig. 11 is a result of enhanced excitation integrated over all wavelengths emitted by the QD. Also, different devices were used in each experiment with varying performance due to fabrication variations and device degradation over the course of experiment trials. In each case, however, the effect of enhanced excitation is evident.

#139110 - $15.00 USD Received 3 Dec 2010; revised 3 Feb 2011; accepted 9 Feb 2011; published 14 Feb 2011

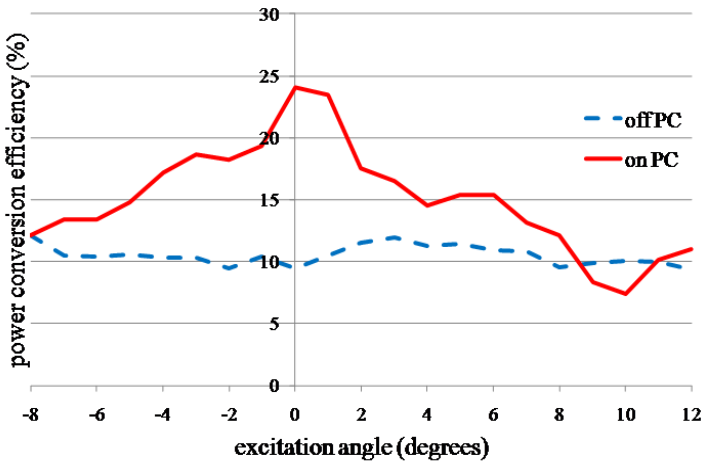

Fig. 11. Power conversion efficiency measured using an integrating sphere and at varying excitation angles. The PC improves the conversion efficiency over 2.5x through the enhanced excitation effect.

6. Conclusion

We demonstrated the design, fabrication, and characterization of a 2D asymmetric PC engineered to improve the conversion efficiency of optical down conversion of PbS QD from the blue to NIR wavelengths. Using a nanoreplica molding process that can potentially scale up to large areas and flexible substrates, we fabricated PC with embedded QD. Both enhanced extraction and enhanced excitation effects were simultaneously possible at wide wavelength separation due to the 2D asymmetric PC design. Coupling to leaky modes of the PC, enabled enhanced extraction effect that preferentially coupled QD emission light out of the PC into controlled directions. This is important for directing light to other optical elements. Furthermore, the enhanced excitation effect was observed when the excitation light was at a resonant condition. This increased the emission intensity and improved the conversion efficiency in comparison to QD embedded in non-structured polymer.

Acknowledgments

The research was supported by BAE Systems IRAD under project manager James M. Ortolf, and the authors acknowledge James M. Ortolf for many helpful discussions.

#139110 - $15.00 USD Received 3 Dec 2010; revised 3 Feb 2011; accepted 9 Feb 2011; published 14 Feb 2011